

Modeling the THz spectrum of the bentazon

Huali Wang (王花丽) and Qiang Wang (王强)*

Department of Quality and Safety Engineering, China Jiliang University, Hangzhou 310018, China

*Corresponding author: qiangwang@cjlu.edu.cn

Received July 1, 2011; accepted August 31, 2011; posted online October 24, 2011

Terahertz (THz) spectra of bentazon are determined within the range of 0.3–2.4 THz at room temperature. Density functional methods are used to compute the THz spectra using three different programs: Gaussian03 for isolated-molecule form, DMol³ and CRYSTAL09 for solid-state forms. Among the three, the computed THz spectrum of CRYSTAL09 shows better bond length and angle agreements with X-ray experimental results, and corresponds with observed THz experiment spectral characteristics. The isolated-molecule vibrational mode values are less by half than those derived from solid-state calculations. The last five peak positions of the two solid-state computations coincide with each other. Moreover, all the experimental THz absorption peaks are assigned by utilizing CRYSTAL09.

OCIS codes: 300.6495, 300.1030, 000.2658.

doi: 10.3788/COL201109.110011.

Bentazon, with chemical name 3-isopropyl-1H-2,1,3-benzothiadiazin-4(3H)-one 2,2-dioxide, is a colorless to slightly brown, odorless crystalline solid. Bentazon is one of the synthetic, contact, and post-emergence herbicide used for selective control of broadleaf weeds and sedges in numerous crop fields.

In recent years, numerous local and foreign investigations have focused on devices and their characteristics^[1,2] as well as on many terahertz (THz)-based substances^[3–5]. Considerable efforts have been made to assign experimental THz spectra^[6–8]. The density functional theory (DFT) and the programs CPMD, CRYSTAL06, DMol³, and Gaussian03 are generally used. The CPMD and CRYSTAL06 are usually used for solid-state system. Gaussian03 is commonly used for molecular form, and DMol³ is employed for molecular and solid forms. However, vibrational intensities for solid-state calculations cannot be obtained from DMol³. Without these intensities, the displayed spectrum can only consist of points on the frequency axis. Therefore, the DMol³ intensity must be roughly calculated^[7]. The assignment of experimental THz spectra continues to be a problem because THz waves are rich in low frequency vibrational modes: crystalline lattice or inter-molecular vibrational modes, hydrogen bonding stretches, and several torsion vibrations. Finding a theory or means to clearly explain THz spectra is difficult.

In the present work, absorption and refractive index spectra of bentazon were obtained in the THz range of 0.3–2.4 THz using the THz time-domain spectroscopy (THz-TDS) system at room-temperature and subsequently purged in nitrogen. Simulation calculations of quantum chemistry programs Gaussian03, CRYSTAL09, and DMol³ were used to analyze vibrational modes. A program to clearly explain the observed THz spectral characteristics is determined by comparing the calculated bond lengths and angles.

Bentazon with 99% purity was purchased from J&K SCIENTIFIC LTD. and used without further purification and treatment. The sample and polyethylene (PE) powder were dried at 310 K for 2 h, and mixed well at 1:1(w/w) ratio. Subsequently, the sample was ground with an agate mortar to minimize particle size.

Approximately 180 mg of the mixture was pressed under 20 MPa into pellets with a diameter of 13 mm and a thickness of 1.424 mm. The THz-TDS experiment setup was based on Ref. [3]. Temperature was approximately 294 K, the optical path of THz was filled with nitrogen, and relative humidity was approximately 3.0%.

Time-domain reference (nitrogen) and sample signals were obtained and averaged by 10 times scans to increase the signal-to-noise ratio (SNR). Approximately 20 ps of time window for reference and sample signals were used with 0.045-THz resolution. The real refractive index $n(\omega)$ and absorption coefficient $\alpha(\omega)$, which respectively described the dispersion and absorption characteristics, were obtained according to the THz band^[9–11], and calculated as

$$n(\omega) = \frac{\phi(\omega)c}{\omega d} + 1, \quad (1)$$

$$\alpha(\omega) = \frac{2}{d} \ln \frac{4n(\omega)}{A(\omega)[n(\omega) + 1]^2}, \quad (2)$$

where ω represents the frequency, d is the sample thickness, c represents the light velocity, $A(\omega)$ is the amplitude ratio of the sample to reference signal, and $\phi(\omega)$ is the relative phase difference.

The first principle calculations based on DFT were obtained using Gaussian03^[12] for the isolated-molecular form. DMol³ (version 4.4) and CRYSTAL09^[13] were employed for the solid-state forms. The B3LYP^[14,15] density function combined with the basis set 6-31G(d,p)^[16] in the Gaussian03 program was used for the isolated-molecular calculations. ULTRAFINE was used as keyword to define the integration grid and atomic positions collected from the optimized crystal structure.

The DMol³ solid-state calculation used “fine” grid sizes (corresponding to a k-point separation of 0.4 nm⁻¹) and convergence criteria ($<10^{-7}$), the double numerical with d and p polarization (DNP) basis set, and Perdew-Wang PWC^[17] local density approximation (LDA). The CRYSTAL09 calculation used hybrid density functions B3LYP and Gaussian-type basis set 6-31G(d,p) to complete the DFT simulation. Total energy convergence criteria $\Delta E < 1 \times 10^{-8}$ hartree for geometrical opti-

mization and $\Delta E < 1 \times 10^{-11}$ hartree for normal mode calculation were used for the DFT process. The TOLINTEG= 8 8 8 16 was set according to Pack-Monkhorst. This controls the truncation criteria of coulomb and HF exchanged integrals as well as SHRINK=4 and intended to generate a commensurate grid of k-points in reciprocal space. XLGRID was a pruned (75,974) grid with 75 radial points and a maximum of 974 angular points in the region relevant for chemical bonding. Atomic positions were optimized within the constraints of fixed unit cell parameter. Infrared (IR) intensities for each normal mode were obtained from dipole moment derivatives based on Born charges as evaluated through Berry phase.

The initial structure of unit cell was obtained from 173-K crystallographic data^[18] for bentazon, space group=P21/c, with parameters $a=1.1658(2)$ nm, $b=0.7406(1)$ nm, $c=1.3296(3)$ nm, $\alpha=90.00^\circ$, $\beta=110.55(2)^\circ$, $\gamma=90.00^\circ$, and $Z=4$. Figure 1 shows the labelled isolated-molecule and crystalline unit cell of bentazon.

Figure 2 shows bentazon from the 0.3–2.4-THz spectra. The average refractive index is 1.492. THz absorption spectra without corrected baselines exhibit four absorption peaks in the effective frequency range. The two strongest absorption intensities are centered at 1.44 and 2.20 THz. A weaker absorption is located at 1.94 THz, and the lowest is situated at 1.80 THz.

Table 1 shows the calculated structural data of bond lengths (left) and bond angles (right) for bentazon from the three programs. The X-ray diffraction and the root-mean-square deviation (RMSD) between the calculated and experimental values are also indicated. The differences in bond length (Fig. 3(a)) and bond angle (Fig. 3(b)) between the calculations and values derived from Ref. [18] are shown.

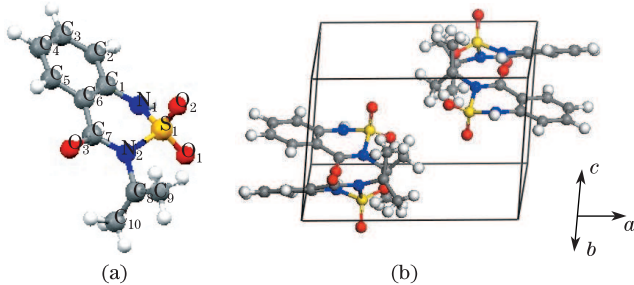


Fig. 1. Structure of (a) isolated labelled bentazon molecule and (b) its solid-state structure.

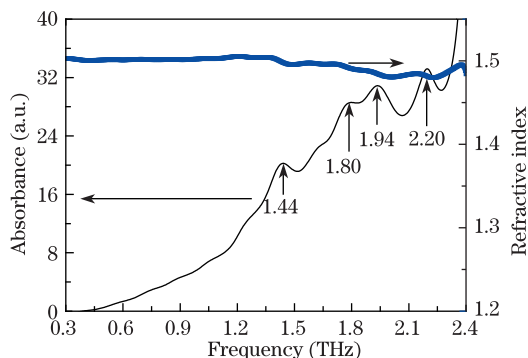


Fig. 2. Experimental THz spectra of bentazon from 0.3–2.4 THz. The arrow points to the corresponding y -coordinate.

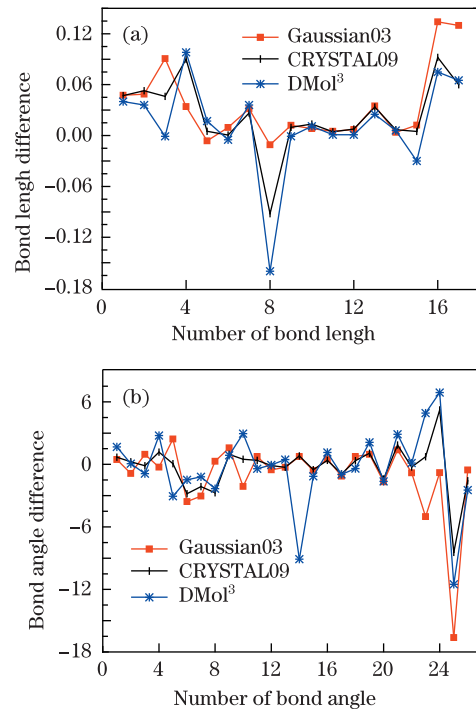


Fig. 3. (a) Bond length and (b) bond angle differences between calculations and the X-ray diffraction results^[18].

Isolated-molecule and solid-state simulations for bond length provide significant similarities with experimental values in term of tendencies. The root mean square deviations (RMSDs) for bond lengths are 0.0552 for Gaussian03, 0.0549 for DMol³, and the slightly better 0.0473 for CRYSTAL09. The relatively obvious bias occurred on the C₈-C₉ from the Gaussian03 simulation with 0.01341-nm deviation, and on the N₂-C₈ from the DMol³ simulation with 0.016-nm deviation. The isolated molecule and solid-state simulations show the same general trend of overestimating or underestimating the bonds, except for bond O₃-C₇. The main reason is the usage of similar, comparable basis sets, wherein the DNP basis set for DMol³ is supposed to be comparable to 6-31G(d,p). The three programs drastically underestimated bond N₂-C₈, which may have been caused by a defect from the basis set or the theory we employed.

A similar trend was found in the calculations for bentazon bond angles. The RMSDs for bond angles of isolated molecule and solid-state simulations are 3.6671 for Gaussian03, 3.6784 for DMol³, and 2.2662 for CRYSTAL09. The relatively obvious bias occurred on the C₉-C₈-C₁₀ from all three programs, with deviations by 16.625° for Gaussian03, 11.511° for DMol³, and 8.44° for CRYSTAL09. The isolated molecule and solid-state simulations demonstrate the same general trend of overestimating or underestimating most bond angles. The bond angle C₉-C₈-C₁₀ was seriously underestimated, which could have been caused by another defect of the basis set or the theory we employed.

Figure 4 is the experimental spectrum plot with the simulated isolated-molecule of bentazon. Frequency (THz) and IR intensity (km/mol) for the calculated IR-active modes are shown in Table 2. The isolated-molecule DFT simulation predicted 3-IR-active vibrational modes for 1.46, 1.71, and 2.36 THz with the corresponding

Table 1. Calculated Bond Lengths and Bond Angles without Hydrogen Atoms for Isolated Molecule and Solid-state Simulations (Exp.=Experiment)

Bond Lengths of Bentazon					Bond Angles of Bentazon					
Bond Lengths	Exp. ^[18]	Gaussian03	DMol ³	CRYSTAL09	No.	Bond Angles	Exp. ^[18]	Gaussian03	DMol ³	CRYSTAL09
S ₁ -O ₁	0.1409	0.1456	0.1449	0.1456	1	O ₁ -S ₁ -O ₂	119.4	119.855	121.078	120.09
S ₁ -O ₂	0.1411	0.1460	0.1447	0.1464	2	O ₁ -S ₁ -N ₁	107.5	106.628	107.562	107.75
S ₁ -N ₁	0.1603	0.1694	0.1602	0.1649	3	O ₁ -S ₁ -N ₂	109.0	109.957	108.104	108.87
S ₁ -N ₂	0.1666	0.1700	0.1764	0.1756	4	O ₂ -S ₁ -N ₁	111.3	111.040	114.071	112.47
O ₃ -C ₇	0.1228	0.1222	0.1245	0.1233	5	O ₂ -S ₁ -N ₂	107.3	109.738	104.246	107.37
N ₁ -C ₁	0.1397	0.1407	0.1392	0.1398	6	N ₁ -S ₁ -N ₂	100.8	97.230	99.322	97.98
N ₂ -C ₇	0.1382	0.1414	0.1418	0.1409	7	S ₁ -N ₁ -C ₁	120.3	117.258	119.100	118.17
N ₂ -C ₈	0.1514	0.1503	0.1354	0.1422	8	S ₁ -N ₂ -C ₇	120.0	120.290	117.665	117.27
C ₁ -C ₂	0.1387	0.1399	0.1386	0.1397	9	S ₁ -N ₂ -C ₈	117.1	118.683	117.966	118.06
C ₁ -C ₆	0.1399	0.1407	0.1410	0.1413	10	C ₇ -N ₂ -C ₈	121.1	118.982	124.050	121.59
C ₂ -C ₃	0.1386	0.1391	0.1387	0.1390	11	N ₁ -C ₁ -C ₂	120.1	120.842	119.684	120.49
C ₃ -C ₄	0.1392	0.1399	0.1393	0.1400	12	N ₁ -C ₁ -C ₆	119.4	118.880	119.339	119.28
C ₄ -C ₅	0.1354	0.1389	0.1379	0.1388	13	C ₂ -C ₁ -C ₆	120.5	120.215	120.962	120.21
C ₅ -C ₆	0.1398	0.1402	0.1404	0.1405	14	C ₁ -C ₂ -C ₃	119.0	119.744	109.904	119.81
C ₆ -C ₇	0.1476	0.1488	0.1446	0.1481	15	C ₂ -C ₃ -C ₄	121.2	120.613	120.046	120.69
C ₈ -C ₉	0.1397	0.1531	0.1472	0.1489	16	C ₃ -C ₄ -C ₅	119.0	119.515	120.139	119.39
C ₈ -C ₁₀	0.1403	0.1533	0.1468	0.1463	17	C ₄ -C ₅ -C ₆	122.0	120.864	121.033	121.08
—	—	—	—	—	18	C ₁ -C ₆ -C ₅	118.3	119.046	117.902	118.65
—	—	—	—	—	19	C ₁ -C ₆ -C ₇	122.0	122.955	124.110	123.07
—	—	—	—	—	20	C ₅ -C ₆ -C ₇	119.6	117.929	117.962	118.20
—	—	—	—	—	21	O ₃ -C ₇ -C ₆	120.5	121.890	123.386	122.35
—	—	—	—	—	22	N ₂ -C ₇ -C ₆	118.4	117.583	118.529	118.14
—	—	—	—	—	23	N ₂ -C ₈ -C ₉	116.1	111.083	121.017	116.83
—	—	—	—	—	24	N ₂ -C ₈ -C ₁₀	113.5	112.705	120.394	118.73
—	—	—	—	—	25	C ₉ -C ₈ -C ₁₀	130.1	113.476	118.589	121.66
—	—	—	—	—	26	O ₃ -C ₇ -N ₂	121.0	120.452	118.529	119.42
RMSD	—	0.0552	0.0549	0.0473	—	RMSD	—	3.6671	3.6784	2.2662

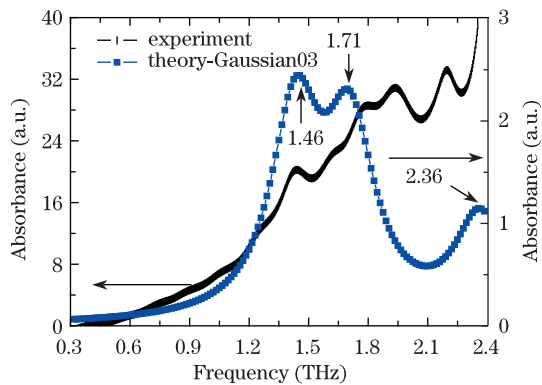


Fig. 4. Comparison of bentazon experimental spectrum with Gaussian03 simulation.

intensities of 1.98, 1.77, and 0.98, respectively. These also correspond to the experimental values of 1.44, 1.80, and 2.20 THz, respectively. The IR-active vibrational modes for 1.46 THz significantly coincide with the 1st experimental peak position 1.44 THz, whereas the 1.71 THz show a 0.09-THz shift from the 2nd experimental value of 1.80 THz. The relatively obvious bias occurred

on the last peak with 0.16-THz deviation. The value is deficient because no simulation value corresponding to the 3rd experimental value of 1.94 THz is obtained.

Figure 5(a) is the plot of the experimental and CRYSTAL09 simulated spectra. The solid-state DFT simulation predicted 8-IR-active vibrational modes for 0.75, 0.96, 1.38, 1.47, 1.57, 1.86, 2.10, and 2.25 THz, with the corresponding intensities of 0.51, 9.54, 0.22, 14.27, 0.11, 4.28, 3.60, and 1.00. The IR active vibrational modes for 1.47, 1.86, 2.10, and 2.25 THz with relatively stronger intensities correspond to experimental values 1.44, 1.86, 1.94, and 2.25 THz, respectively. A larger shift of 0.16 THz occurred at the experimental value of 1.94 THz. The simulation of all the experimental values is partly successful, although irrelevant values may have been introduced.

Figure 5(b) is the plot of the experimental and DMol³ simulated bentazon spectrum. The solid-state DFT simulation of DMol³ predicted 7-IR-active vibrational modes for 1.07, 1.12, 1.46, 1.55, 1.80, 2.05, and 2.27 THz, with the corresponding intensities of 2.32, 0.69, 0.47, 2.71, 3.35, 0.35, and 1.62. The IR-active vibrational modes for 1.46, 1.80, 2.05, and 2.27 THz correspond to

Table 2. Vibrational Mode Description of the CRYSTAL09 Simulation

Mode	Experiment	CRYSTAL09	Intensity	Mode Description
d	1.44	1.47	14.27	External Rotation Along b Axis
f	1.80	1.86	4.28	Benzene Ring ($C_1 \cdots C_6$) Along a Axis and C_8 - C_9 Torsion
g	1.94	2.10	3.60	Benzene Ring ($C_1 \cdots C_6$), C_8 - C_9 Torsions
h	2.20	2.25	1.00	C_9 - C_8 - C_{10} Torsion

Table 3. Frequency (THz) and IR Intensity (km/mol) for Calculated IR-active Modes of Bentazon

Mode	Experiment	Isolated-molecule		Solid-state			
		Gaussian03		CRYSTAL09		DMol ³	
		Frequency	Intensity	Frequency	Intensity	Frequency	Intensity
a	—	—	—	0.75	0.51	—	—
b	—	—	—	0.96	9.54	1.07	2.32
c	—	—	—	1.38	0.22	1.12	0.69
d	1.44	1.46	1.98	1.47	14.27	1.46	0.47
e	—	—	—	1.57	0.11	1.55	2.71
f	1.80	1.71	1.77	1.86	4.28	1.80	3.35
g	1.94	—	—	2.10	3.60	2.05	0.35
h	2.20	2.36	0.98	2.25	1.00	2.27	1.62

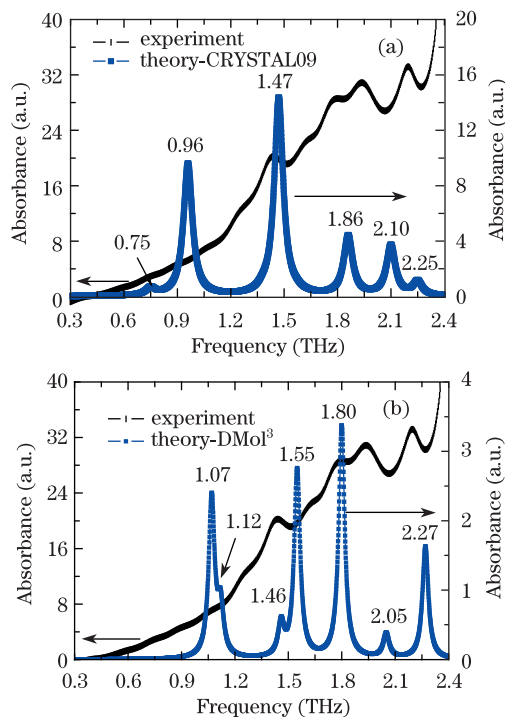


Fig. 5. Comparison of bentazon experimental spectrum with the solid-state simulation of (a) CRYSTAL09 and (b) DMol³.

experimental values 1.44, 1.80, 1.94, and 2.20 THz, respectively. The IR-active vibrational modes for 1.80 THz significantly coincide with the 2nd experimental peak. A bigger shift of 0.11 THz occurred at the experimental value of 1.94 THz. All four peak positions show slight differences with the experimental peak positions. However, the peak positions at 1.46 and 2.05 THz have significantly weak intensities of 0.47 and 0.35, respectively.

The assignment of IR-active vibrational modes com-

prising the experimental bentazon spectrum is derived from the solid-state DFT simulation of CRYSTAL09, which is qualitatively determined by inspecting normal mode displacement eigenvectors. The vibration modes predicted in the THz range consist mainly of internal and external motions. Generally, the internal modes include the torsions of benzene ring, methyl, and chain, whereas the external modes include the molecular translation and molecular rotation, etc. Table 2 shows the detailed mode description of CRYSTAL09 simulation. Mode d originates from the external rotation along the b axis; mode f from the benzene ring ($C_1 \cdots C_6$) along the a axis and C_8 - C_9 torsion; mode g from the benzene ring ($C_1 \cdots C_6$) and C_8 - C_9 torsions; mode h from the C_9 - C_8 - C_{10} torsion.

Table 3 shows the DFT predicted frequencies and intensities of bentazon. Modes a, b, c, e, and g are absent in the Gaussian03 simulation, mainly due to the isolated-molecule DFT simulation which do not consider the action of intermolecular and crystal lattice, etc. The CRYSTAL09 solid-state simulation coincides with the experimental spectrum because the calculated bond lengths and angles conform to X-ray diffraction results better. The last 5 peak positions of the DMol³ simulation coincide with the last 5 peak positions of the CRYSTAL09 simulation. However, their intensities differ, which may have been caused by our rough calculations for the DMol³ intensities or the program itself. Comparing the calculations and experimental structure with X-ray diffraction results in Ref. [16], temperature is found to be a significant factor for bond length and angle differences. The temperatures used differed from each other and from the X-ray diffraction temperature.

Gaussian03 was employed to model single and isolated molecule that does not conform to the experimental form. The THz spectra of bentazon and solid-state periodic system involved intramolecular or phonon interactions. Theoretically, the solid-state calculation is

more reasonable. Generally, the number of IR-active vibrational modes for the isolated-molecule simulation is significantly lesser than that of the solid-state simulation.

THz spectra of bentazon, including refractive index and absorption coefficient, are determined from 0.3–2.4 THz at room temperature. Quantum chemistry calculations are used to analyze isolated-molecule and solid-state vibrational modes. Among the three programs, the solid-state simulation of CRYSTAL09 presents bond lengths and angles that theoretically coincide with the observed X-ray diffraction structures and THz-TDS results at room temperature. Therefore, an optimized structure decides the calculated absorption spectrum. Enhancing the agreement of the optimized structure with X-ray diffraction results or actual structure increases the agreement between the calculated THz spectrum and the experimental THz absorption spectrum. The program CRYSTAL09 is an effective means of modeling THz spectrum and in assigning the absorption peaks of crystal substances.

This work was supported by the National Quality Supervision and Inspection Public Welfare Project of China (No. 200910181) and in part by the National Natural Science Foundation of China (No. 60902095).

References

1. J. Gu, Z. Tian, Q. Xing, C. Wang, Y. Li, F. Li, L. Chai, and C. Wang, *Chin. Opt. Lett.* **8**, 1057 (2010).
2. Y. He, Y. Jiang, Y. Zhang, and G. Fan, *Chin. Opt. Lett.* **8**, 162 (2010).
3. Y. F. Hua, H. J. Zhang, and H. L. Zhou, *IEEE Trans. Instrum. Meas.* **59**, 1414 (2010).
4. S. Wietzke, C. Jansena, F. Rutz, D. M. Mittleman, and M. Koch, *Polym. Test.* **26**, 614 (2007).
5. H.-B. Liu, Y.-Q. Chen, G. J. Bastiaans, and X.-C. Zhang, *Opt. Express* **14**, 415 (2006).
6. Y. Zhang, X.-H. Peng, Y. Chen, J. Chen, A. Curioni, W. Andreoni, S. K. Nayak, and X.-C. Zhang, *Chem. Phys. Lett.* **452**, 59 (2008).
7. D. G. Allis, D. A. Prokhorova, and T. M. Korter, *J. Phys. Chem. A* **110**, 1951 (2006).
8. M. D. King, P. M. Hakey, and T. M. Korter, *J. Phys. Chem. A* **114**, 2945 (2010).
9. T. D. Dorney, R. G. Baraniuk, and D. M. Mittleman, *J. Opt. Soc. Am. A* **18**, 1562 (2001).
10. L. Duvillaret, F. Garet, and J.-L. Coutaz, *IEEE J. Sel. Top. Quantum Electron.* **2**, 739 (1996).
11. L. Duvillaret, F. Garet, and J.-L. Coutaz, *Appl. Opt.* **38**, 409 (1999).
12. M. J. Frisch, G. W. Trucks, and H. B. Schlegel, *Gaussian 03 (Revision9C. 02 Gaussian, Inc.)* (Wallingford, CT, 2003).
13. R. Dovesi, V. R. Saunders, and C. Roetti, *Crystal09 User's Manual* (University of Torino, Torino, 2009).
14. A. D. Becke, *J. Chem. Phys.* **98**, 5648 (1993).
15. P. J. Stephens, F. J. Devlin, C. F. Chabowolski, and M. J. Frisch, *J. Phys. Chem.* **98**, 11623 (1994).
16. P. C. Hariharan and J. A. Pople, *Theor. Chim. Acta.* **28**, 213 (1973).
17. J. P. Perdew and Y. Wang, *Phys. Rev. B* **45**, 13244 (1992).
18. L. E. Moss, B. A. Karcher, J. W. Richardson, and B. A. Jawbson, *Acta. Crys. C* **42**, 1785 (1986).